Microchemical Journal 175 (2022) 107186

Contents lists available at ScienceDirect

Microchemical Journal

journal homepage: www.elsevier.com/locate/microc

Speciation of organoarsenicals in aqueous solutions by Raman spectrometry and quantum chemical calculations

R. López [a,1,*], F.J. Pereira [a,1], D. Suárez [b], A.J. Aller [a]

[a] Department of Applied Chemistry and Physics, Faculty of Biological and Environmental Sciences, University of León, Campus de Vegazana, s/n, E-24071 León, Spain
[b] Department of Physical and Analytical Chemistry, Area of Physical Chemistry, Faculty of Chemistry, University of Oviedo, Julián Clavería 8, E-33006 Oviedo, Spain

ARTICLE INFO

Keywords:
Organoarsenicals
Speciation
Qualitative identification
Raman spectrometry
Density Functional Theory
Computational Chemistry

ABSTRACT

Knowledge about the existence and stability of different species of organoarsenicals in solution is of the most significant interest for fields so different as chemical, environmental, biological, toxicological and forensic. This work provides a comparative evaluation of the Raman spectra of four organoarsenicals (*o*-arsanilic acid, *p*-arsanilic acid, roxarsone and cacodylic acid) in aqueous solutions under acidic, neutral and alkaline conditions. Speciation of some of these organoarsenicals is possible by Raman spectrometry at different selected pHs. Further, we examine the proficiency of computational chemistry to obtain the theoretical Raman spectra of the four organoarsenicals compounds. To this end, we employ a computational protocol that includes explicit water molecules and conformational sampling, finding that the calculated organoarsenicals spectra agree reasonably well with those experimentally obtained in an aqueous solution in the whole pH range covered. Finally, we highlight the effectiveness of quantum chemical calculations to identify organoarsenicals in an aqueous solution.

1. Introduction

Arsenic compounds are very toxic, although they have also shown some practical biological and clinical applications based on their inhibitory activity towards thioredoxin reductase [1] and the treatment of diverse illnesses, such as syphilis [2,3], sleeping sickness [4], and different types of cancer [5] such as promyelocytic leukaemia [6,7]. Some aromatic organoarsenicals, including 3-nitro-4-hydroxy-phenylarsonic acid (roxarsone) and amino-phenylarsonic acids (arsanilic acids), are very useful as antimicrobials, many times added as feed additives, particularly in seafood [8]. Other non-aromatic organoarsenicals, such as cacodylic acid (dimethylarsinic acid), are widely involved in veterinary medicine due to their use as herbicides and defoliants [9], which usually generate immediate environmental problems. Furthermore, the living organisms mainly release organoarsenicals into the environment because they methylate the inorganic arsenic species, while other times, they excrete organoarsenicals unchanged. All organoarsenic compounds show potential health impact [10], although their degradation products may also generate higher toxicity [11–13]. Thus, non-volatile methyl arsine oxides, such as methyl-arsonic acid and cacodylic acid, are found in different environmental systems, enhancing the toxicological risks [14–20]. The chemical stability of organoarsenicals depends on the Eh-pH conditions of the environment, although on many occasions, they degrade to inorganic arsenic, increasing the pollution problems significantly. Consequently, accurate knowledge about the behaviour of these compounds in aqueous media at different pHs is of concern to clarify emerging different biogeochemistry processes and toxicological studies. Thus, the elucidation of the possible structural changes with pH is interesting for understanding potential toxicity and degradation mechanisms.

Separation and detection of these organoarsenicals rely mainly on techniques like liquid chromatography-mass spectrometry (LC-MS) and inductively coupled plasma-mass spectrometry (ICP-MS) [10,21,22], even though other methodological developments have also evolved as valuable alternatives for determining different species of arsenic [22–27]. However, these techniques are usually costly, sample destructive, and require complex and time-consuming operational protocols. Hence, the development of simple, nondestructive, and information-rich detection approaches is mandatory for the rapid and cost-effective detection of organoarsenicals. In this line, molecular techniques are adequately advantageous for this purpose, being the vibrational spectroscopies [28] well-accepted tools for analysing diverse

* Corresponding author.
E-mail address: rlopg@unileon.es (R. López).
[1] R. López and F.J. Pereira contributed equally.

https://doi.org/10.1016/j.microc.2022.107186
Received 12 November 2021; Received in revised form 4 January 2022; Accepted 5 January 2022
Available online 8 January 2022

types of compounds in any aggregation state [29,30]. Raman spectrometry is probably the best option to work with aqueous solutions because water is a bad Raman scatter, thus providing an interfering-free broad wavenumber region, usually with very isolated peaks, which extend below 400 cm^{-1}. Raman spectrometry is also particularly adequate due to the possibility of working with minimal or even no previous samples preparation.

On the other hand, modelling the Raman spectra of the organoarsenicals helps better understand the chemical and structural nature of the organoarsenicals, improving and predicting knowledge about their behaviour in solution. The theoretical prediction of Raman spectra mainly involves using database lookups, neural networks and other prediction softwares. However, these programmes work well to model molecules with common functional groups but provide unreliable results for complex molecules with unusual functionalities, like organoarsenicals. Reasons for this inconsistency refer to the use of gas-phase molecules in simulation. Therefore, using a reliable environment for organoarsenicals spectra simulation is a challenging problem to solve. In this matter, spectroscopic calculations based on *ab initio* Molecular Dynamics simulations in explicit solvent eventually provide reliable predictions [31], but, on the other hand, they are still computationally expensive for being applied to organoarsenic species. In this context, successful applications of DFT methods are usual in Raman spectra calculations of arsenic-containing species [32–34] with a lower computational cost. Thus, the prediction of Raman parameters based on quantum chemical methods, especially DFT, can be a reliable procedure to estimate relevant molecular properties, even for complex arsenic compounds [35,36], which helps to understand the chemistry and Raman spectroscopy of organoarsenicals [37]. In this respect, we have recently proposed a DFT computational protocol that includes both explicit water molecules and a solvent continuum to predict the Raman spectra of $As^{(V)}$ and $As^{(III)}$ oxoacids in solution [38]. As the performance of such approach is quite satisfactory for the inorganic species, we pursue the challenge to compare the experimental and theoretical spectra in organic molecules with different functional groups.

This work compares the experimental Raman spectra of various organoarsenicals (*o*-arsanilic acid, *p*-arsanilic acid, roxarsone and cacodylic acid) in an aqueous solution at different pHs with the theoretical Raman spectra predicted by coupling a DFT representation of the solutes and selected water molecules to an implicit solvent model of the bulk solvent. Focusing on the Raman peaks of the organoarsenic groups, we discuss the results according to the pH-dependent molecular chemistry and the theoretical modelling of their Raman frequencies in solution.

2. Experimental

2.1. Chemicals

Chemicals of analytical reagent grade were from Merck (Darmstadt, Germany). Sample solutions were prepared in distilled/deionised water (18 MΩcm). All organoarsenicals (*o*-arsanilic acid, *p*-arsanilic acid, cacodylic acid and roxarsone) (99%) were from Sigma-Aldrich (Burlington, MA, United States).

2.2. Methods

All As solutions, concentrated and diluted, were firstly alkalinised with NaOH (0.5 M) up to very alkaline conditions (pH ≈ 12.0). Then, the alkalinised aqueous solutions (pH ≈ 12.0) were acidified by adding HCl (0.5 M) under continuous stirring until the achievement of the desired pH. According to the Eh-pH diagram, we selected the pH values to facilitate the prevalent organoarsenicals species at each pH (Fig. S1). Thus, the following nominal pH values were 12.0, 9.5, 6.0, 3.0 and 0.5. The pH values were adjusted just before the Raman spectroscopic recordings using a pH meter Mettler Toledo (Columbus, Ohio, USA) with a glass electrode.

2.3. Instrumentation

The Raman spectra were acquired by a BWTEK portable Raman spectrometer (Newark, DE, USA), *i*-Raman model, fitted with a refrigerated CCD detector and the 785-nm line laser, CleanLaze model (300 mW) as the excitation source. As in our previous works [38], we used the standard experimental conditions to record the spectra between 150 and 3300 cm^{-1} in the backscattering geometry at room temperature. The results were processed using the Origin 9.0 software (Origin Lab Corporation, Northampton, MA, USA). To increase the signal-to-background ratio of the Raman spectra, we deposited aliquots of 5 μL of the pH-stabilised organoarsenicals aqueous solutions on golden plate supports.

2.4. Computational studies

As previously mentioned, we have recently used and validated a procedure [38] to explore the prediction of the Raman spectra of $As^{(V)}$ and $As^{(III)}$ oxoacids in solution by coupling a DFT representation of the solutes and the closest water molecules to an implicit solvent model of the bulk solvent. Consequently, we only highlight the most relevant characteristics of the computational protocol (further details can be found elsewhere [38]).

According to preliminary benchmark, calculations carried out *in vacuo* on a set of small species, [38] the B3LYP [39,40] functional in combination with the Dunning's double (aug-cc-pVDZ) or triple-ζ (aug-cc-pVTZ) [41–43] basis sets, yields reasonably accurate harmonic frequencies. For brevity, we designate these basis sets as CVDZ and CVTZ. Unfortunately, arsenic-containing molecules have not been considered in the benchmark studies. Kesharwani and Sinha [44,45] aimed to derive single scaling factors (*f*) in order to improve the quality of harmonic force constants determined at medium or low levels of theory. Therefore, decided to derive such scaling factors basing on the experimental data for the test molecules, but it turns out that at least two factors are required for a satisfactory correction: $f_{<900} = 1.0103$ / $f_{>900} = 0.9749$ at B3LYP/CVTZ and $f_{<900} = 1.0240$ / $f_{>900} = 0.9826$ at B3LYP/CVDZ. The scaling factor, $f_{<900}$, acts as a *specific* correction affecting the stretching/bending motions of the As-O bonds while $f_{>900}$ is basically a global scaling factor, whose numerical value (~0.98) is similar to those available in the literature. This strategy is in consonance with more sophisticated approaches [46] that employ different scaling factors for different types of force constants and different functional groups.

We first optimise the molecular geometries of the isolated organoarsenic species at the B3LYP/CVTZ and B3LYP/CVDZ levels of theory combined with the Polarisable Continuum Model (PCM) in the integral equation formalism (IEF) [47,48] by using the *Gaussian16* package. [49] The B3LYP function improved with the third-generation pairwise dispersion correction (D3) with the Becke-Johnson rational damping function [50,51]. After conducting frequency calculations on the optimised geometries, the Raman spectra were obtained within the PCM framework [52], including thus continuum-solvent effects on the harmonic frequencies.

In addition, we also obtained the maximum surface electrostatic potential ($V_{S,max}$) on the acidic hydrogen atoms of the organoarsenic compounds, given that this electrostatic descriptor correlates with the relative acidity in terms of the pK_a values of many compounds [53,54]. The pK_a differences in the organoarsenic species reflect their inductive and mesomeric effects, which we further characterise in terms of the delocalisation index (DI) as a covalent bond order descriptor. The DI derived from Quantum Chemical Topology (QCT) by integrating the exchange–correlation density $\rho_{xc}(\mathbf{r_1},\mathbf{r_2})$ over the topological atomic basins from the charge distribution $\rho(\mathbf{r_1})$. It measures unambiguously the number of electrons shared between two atoms in a molecule, detects

subtler bonding effects and directly relates with the energy associated with the given interatomic interaction [55]. We achieved the DI values and the total charges within the atomic basins with the PROMOLDEN code [56] using the B3LYP/CVTZ density.

To incorporate the effects on the Raman spectra due to explicit water molecules and conformational motions, we considered a hybrid solvent model, which includes a few explicit water molecules in the first hydration shell around arsenic groups, in such a way that the solvent continuum surrounds the solute and the selected waters. To build these models, we carried out a classical Molecular Dynamics (MD) simulation (1.00 *ns*) of each solute embedded within a 25 Å spherical cap of TIP3P [57] water molecules, using the GAFF force field to represent the solute species [58,59]. The parameterization of the solute molecules was carried out using the antechamber software included in the AMBER18 package [59]. The bonded parameters to treat the As atoms were adapted from those available for P while the vdW parameters were taken from the universal force field [60]. Atomic charges for the solute atoms were derived from the B3LYP/aug-cc-pVTZ electrostatic potential using the RESP methodology as implemented in antechamber. MD simulations were run using the SANDER program included also in AMBER18. The time step of the MD simulations was 1.0 fs, and the SHAKE algorithm constrained all the bond lengths at their equilibrium values. A non-bond pair-list cut off of 15.0 Å was used, maintaining the temperature at 300 K using Berendesen's algorithm. We selected fifty equally-spaced MD snapshots from each trajectory, post-processed to remove all water molecules except the two closest ones around those atoms belonging to the arsenic groups. Because of their high computational cost, the resulting models were optimised at the PCM-B3LYP/CVDZ level of theory, followed by harmonic frequency calculations and Raman scattering activity calculations. We used the Multiwfn [61] software to transform the Gaussian output files into theoretical spectra convoluting peak intensities with a Lorentzian function, with a full width at half maximum (FWHM) of 4 cm^{-1}. At last, we averaged the resulting cluster spectra to obtain the final Raman spectrum of each solute at the varying pH.

2.4.1. Arsenic speciation calculations

For comparison with experimental results, we obtained pH-averaged spectra based on the computational spectra of the various species and the experimental data about p*K*a values, pH values and ionic strengths. We averaged the spectra using the fractional concentrations of the various compounds in equilibrium at the given pH.

As previously explained, we adjusted the pH with an acid solution of HCl 0.5 M and a basic solution of NaOH 0.5 M. We tried first to use the Pitzer equations [62] to obtain the chemical compounds' activity coefficients in equilibria at each pH value. However, to the best of our knowledge, up to date, there are no experimental data to apply the Pitzer equation for covering the protomers of the species of interest in this manuscript in the whole pH experimental range. For example, Yang et al. [63] studied some inorganic arsenic oxoacids as the system $H_3AsO_4/H_2AsO_4^-$ in NaCl solutions. Millero et al. [64] studied some arsenic deprotonations in marine waters. On the Pitzer model uses, Simoes et al. estimated the Pitzer parameters for 1–1, 2–1, 3–1, 4–1 and 2–2 single electrolytes [65]. However, more recently, May and coworkers [66] pointed that this (and similar) estimation methods consider only the simple reactant species (*e.g.*, metal and ligand ions), and they fail to address the product species (*e.g.*, complexes), which represent the main challenge. Consequently, we used the Davies equations to calculate the activity coefficients of the species in each deprotonation equilibrium and, subsequently, their relative abundances at different pH values.

3. Results and discussion

3.1. General comments about organoarsenicals

Three of the four organoarsenicals compounds used in this study involve the arsonic group, -As(=O)$(OH)_2$, joined to a benzene ring substituted by hydroxyl (–OH), nitro (–NO_2) and amino (–NH_2) groups in different positions depending on the organoarsenicals considered. However, the fourth compound, cacodylic acid, contains the arsinic group R_2−As(=O)(OH) joined to two methyls (R: –CH_3) chains. The arsonic and arsinic groups contain a proton donor part (As−OH) and a proton acceptor group (As=O), which facilitates the formation of hydrogen-bonded self-association [67], particularly under acidic conditions. The four organoarsenicals show a few similar Raman bands (Figs. 1-4A, B, Table 1) due to the arsonic/arsinic group contribution, although mediated by the other parts of the molecule and pH conditions (Table 2 and Table S1).

To a closer description, we obtained the $V_{S,max}$, DI and QCT charges of each atom of the molecules (*Q*) and presented them in Supplementary Information-2. As a whole, the $V_{S,max}$ and the experimental pK_a correlate well for the three compounds with the arsonic group $\left(pK_a = -0.054 \cdot V_{s,max}(kcal/mol) + 6.86\right) \therefore R^2 = 0.979$), showing thus that $V_{S,max}$ is a reliable p*K*a descriptor for the arsenic group. Other results result by assessing the functional groups' electronic effects in the molecules studied. These effects are pH-dependent and can be categorised as (i) electron-withdrawing: (-*I*: –NO_2, –OH, -AsO_3H_2, –NH_2, –NH_3^+) or (-*M*: –NO_2, -AsO_3H), and (ii) electron-donating: (+*I*: -AsO_2^-, -O^-) or (+*M*: –OH, –NH_2, -O^-). Thus, for the arsanilic acids, the nitrogen atom in the amino group (–NH_2) participates as a donating group by conjugation (+*M*) through its free electron pair in resonance with the benzene ring. Certainly, we observed the resonance effect in our DI calculations: in *o*-arsanilic acid, the DI between the nitrogen atom (atom no. 7) and the carbon atom to which it is connected (atom no. 5) is 1.12, higher than a rigorous single bond (DI = 1) and close to the DI between the carbon atoms of the aromatic ring (*e.g.* C(5)-C(4) = 1.27, C(5)-C(6) = 1.26). In the *p*-arsanilic acid, these indexes are very similar (see Supplementary Information-2) (N(7)-C(6) = 1.10 vs. C(6)-C(1) = 1.27, C(6)-C(6) = 1.26).

Simultaneously, the amino group acts as an inductive electron-withdrawer group (-*I*) due to the higher electronegativity of a nitrogen atom against a carbon atom. However, suppose the free electron pair of this amino group is disabled. In that case, it cannot participate in conjugation through resonance, as occurs for the primary ammonium ion (–NH_3^+) present under strongly acidic conditions, only showing a negative inductive effect and retrieving electrons from the aromatic ring. Our calculations assess this effect by considering the DI between the nitrogen and carbon atoms connected in the aromatic ring. Of course, when the ammonium ion (–NH_3^+) is present, the DI falls from 1.12 to 1.10 in *o*-arsanilic acid and *p*-arsanilic acid with the amino group respectively to ~ 0.93. Therefore, we can confirm that the conjugative effect disappeared under strongly acidic conditions.

Further, when the amino group acts as an electron-donating group through conjugation, this mesomeric effect masks the existing inductive withdrawing effect. Both the *ortho*- and *para*- arsanilic acids activate the benzene ring by the resonance effect according to the selected DI values (i.e., the C-N DI in *ortho*- and *para*- position is 1.12 and 1.10, respectively). Although this effect increases slightly in the *ortho*- position, the lower pK_a of the *o*-arsanilic acid concerning *p*-arsanilic is most likely due to the presence of an intramolecular H-bond between the –NH_2 and –$AsO(OH)_2$ moieties, which can facilitate the dissociation of the acidic O–H bond (Figs. 1-4A). We can assess the relevance of such H-bond through the DI value (0.08) between the hydrogen of the amino group, closer to the arsonic group, and the oxygen atom of As=O. This value is higher and far from other noncovalent interactions. In a closer inspection, we checked the numerical value of this descriptor in the conjugated

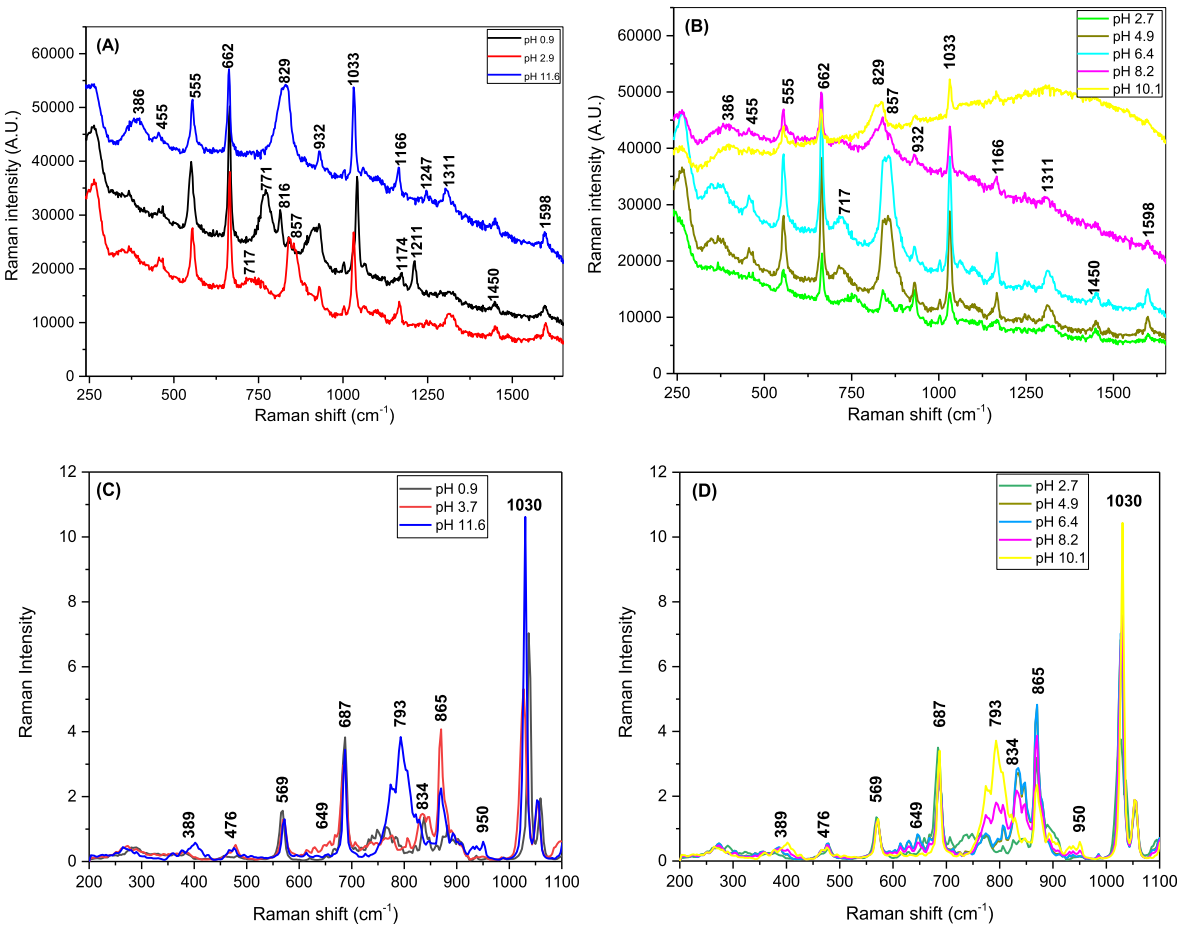

Fig. 1. Raman experimental (A, B) and computational (C, D) spectra of the *o*-arsanilic acid solutions at different pHs.

base of *o*-arsanilic acid, and we found a more significant DI value (0.10). Therefore, the H-bond formed between the amino and the arsonic groups, only in *o*-arsanilic acid, explains well the more considerable acidity of this compound than that of the *para* isomer.

Contrarily, roxarsone shows the opposite behaviour. The reason is that the nitro group (–NO_2) in roxarsone, in *meta*-position concerning the arsonic group, acts as an electron-withdrawing group, favouring the dissociation of the –OH bond in the arsonic group. The result is that the acidic character of the arsonic group increases, decreasing its pK_a value. We can also characterise this electron-withdrawing behaviour by our net charge calculations reported in Supplementary Information-2. As a whole, the nitro group (–NO_2) in roxarsone presents a negative charge of −0.58 e^-. For the sake of comparison, the amino group (–NH_2) in *o*-arsanilic acid and *p*-arsanilic acids are −0.30 and −0.31 e^-, respectively. Consequently, the net charge in the arsonic group becomes + 0.17 e^- in roxarsone vs + 0.12 and + 0.10 e^- in *ortho*- and *para*- arsanilic acid, respectively. Regarding the electrostatic potential, assessment of the electron-withdrawing character is also possible by the $V_{S,max}$ on the acid hydrogen atoms of the arsonic group. These values are 55.9 and 50.7 kcal/mol in *ortho*- and *para*- arsanilic acid vs 63.4 kcal/mol of roxarsone. Finally, the DI of the acid (–OH) group in the arsonic group decreases from 0.59 in arsenic acids to 0.58 in roxarsone. As a result, these descriptors directly compare the compounds' acidic character with the arsonic group: roxarsone > *o*-arsanilic acid > *p*-arsanilic acid.

Considering that a nitro group is an electron-withdrawing group in *meta*-, and the -O- and –OH groups are electron-withdrawing groups in *ortho*- and *para*-, both contributions are balanced, at least partially from a quantitative point of view. Albeit the previous discussion, the phenolic hydroxyl group in *ortho*- or *para*- positions, concerning the nitro group in roxarsone, decreases its electron density, thus increasing its acidic character with a pK_a value (pK_a = 9.76) smaller than phenol (pK_a = 10.02). On the other hand, the methyl groups are electron donors, facilitating dissociation of the arsinic group in cacodylic acid (smaller pK_a = 6.14). These considerations help understand possible alterations in the Raman shifts of the arsonic and arsinic acids and the other functional groups. Further, the formation of different hydrogen bridges is reasonable in the aromatic compounds but differently depending on the pH value selected (see Table 2).

In the set of the theoretical spectra, the range of frequencies in Figs. 1-4 C, D goes from 200 to 1100 cm^{-1}. One reason to truncate the experimental frequency range for calculations is the possibility of identifying the selected organoarsenicals through the arsonic and arsinic acid groups in the frequency range of 600–900 cm^{-1}. Over 1100 cm^{-1}, the most remarkable contributions to the spectra peaks are mainly about functional groups (*e.g.*, NO_2 or –NH_2) that are not associated with vibrations of the arsenical groups, and, therefore, they are out of vital interest in this study. Therefore, to keep the computational cost of the DFT calculations within tractable bounds, only the arsonic and arsinic groups were "micro-hydrated" by explicit water molecules in the corresponding cluster models.

A general inspection of the theoretical spectra (see Figs. 1-4 C, D) show a good agreement with the experimental ones (Figs. 1-4 A, B) in the prominent peaks in both shape and position, validating the utility of the hybrid DFT approach. However, the limited amount of conformational sampling, the lack of anharmonicity effects in the spectra calculations and the intrinsic deficiencies of the B3LYP/CVDZ level of theory would be behind differences found between experimental and the theoretical spectra. More particularly, the DFT spectra of the aliphatic organoarsenicals (*o*-arsanilic acid, *p*-arsanilic acid and roxarsone) present a systematic overestimation of the vibrational frequencies

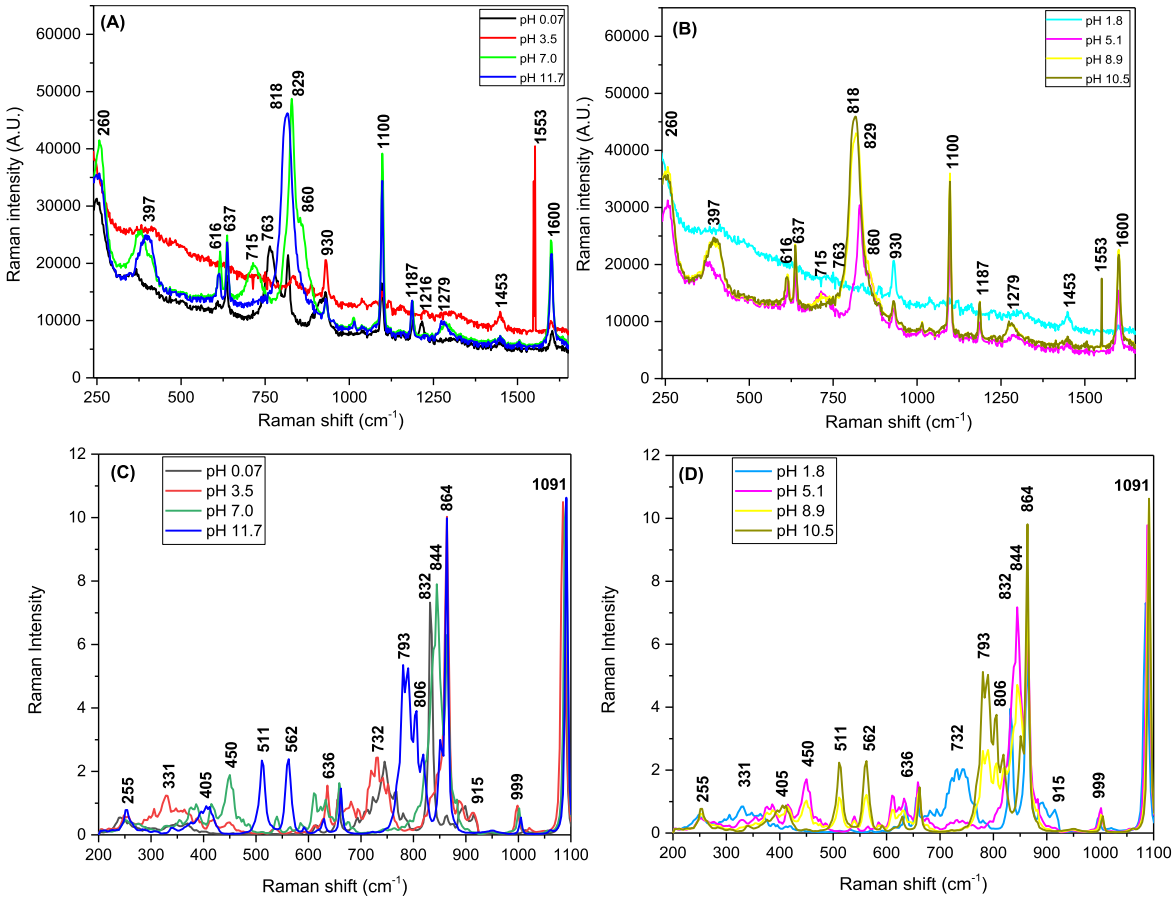

Fig. 2. Raman experimental (A, B) and computational (C, D) spectra of the *p*-arsanilic acid solutions at different pHs.

(~0.5–2.0%) whilst the cacodylic acid, a smaller molecule with an arsinic group, presents an underestimation of the frequencies (~0.5–2.7%) (see below).

A close inspection of the optimised cluster models shows that the water molecules form a network of H-bond interactions with the arsenic/arsenic atoms and vicinal groups (–NH_2, –OH). In this sense, we found that H-bonds maximise along with the geometry optimisation calculations by the reorientation of the water molecules. A visual inspection of some clusters of the neutral solutes (see Figs. S2-S5) anticipates that the solute O, H and N atoms, with 1~3H-bonds each, can present an essential contribution to the broadening of the spectra peaks confirmed in our previous work [38]. We obtained the percentage weight of water coordinates in the harmonic vibrational modes for the cacodylic acid (Table S2). Thus, Table S2 confirms the existence of an essential water-solute coupling for the anionic cacodylic acid (~34% average), higher than for the neutral protomer of the cacodylic acid (~25% average).

3.2. *Effect of pH on the Raman spectra of organoarsenicals*

We obtained the Raman spectra of the different organo-$As^{(V)}$ species in solution, at different pHs, selected according to the Eh-pH and pH fractional composition diagrams (Figs. 1-4 A, B). For some of the pHs selected, several As species can coexist, potentially deforming the shape of the Raman peaks and suffering slight shifts of the maximum. Similarly, the theoretical spectra of these organoarsenicals appear in Figs. 1-4 C, D.

The organo-$As^{(V)}$ compounds' spectroscopic characterisation uses mainly the Raman bands assigned to the As–O and As–OH vibrations according to the theoretical symmetry considerations of the organo-$As^{(V)}$ compounds. The Raman experimental spectra of the four organoarsenicals compounds related to a particular species are in Figs. 1-4 A, B. Further, Table 1 shows all the Raman experimental bands found at any pH for the four organoarsenicals and the corresponding assignment. Identification of organoarsenicals is possible through the arsonic and arsinic acid groups, exhibiting several Raman modes in the 600–900 cm^{-1} range. The Raman experimental spectra of the arsanilic acids (Table 1) show the symmetric and asymmetric stretching modes for As = O in the region 800–900 cm^{-1}; the As−OH asymmetric stretching mode at 700–800 cm^{-1} and the stretching modes at 616 cm^{-1} and 640 cm^{-1} assigned to As–C. The bands of the arsonic acid group agree in the main with the results provided by other works also using conventional Raman studies [35]. In the theoretical spectra shown in Figs. 1-4 C, D, the motions As=O and As-OH are in the same region of the experimental data. However, overestimation of the more concise assignments of symmetric and asymmetric stretching frequencies of As-C averages an ~ 2.4% in the case of solutes with an aromatic ring, while an underestimation of 0.99% results in the case of cacodylic acid.

Some alternative bands relate to the other functional groups existing in the molecules selected and can serve as specific markers for these compounds. Thus, the NH_2 group in arsanilic acids decreases the Raman shifts with electron-withdrawing groups (-AsO_3H_2) in *para*- position (*p*-arsanilic acid) because the *p*-π resonance effect between the amino group and benzene ring grows. No readily identifiable peaks appear in *p*-arsanilic acid for the amine group, and the contrary occurs with electron-donating groups. For *o*-arsanilic acid, however, usually incorporating an additional cyclic structure resulting from an intramolecular hydrogen bond, drastically changes its spectroscopic behaviour, including a Raman shift at 1311 cm^{-1} assigned to $\nu_s(NH_2)$.

The NO_2 group in roxarsone shows peaks at 1332 and 1356 cm^{-1}

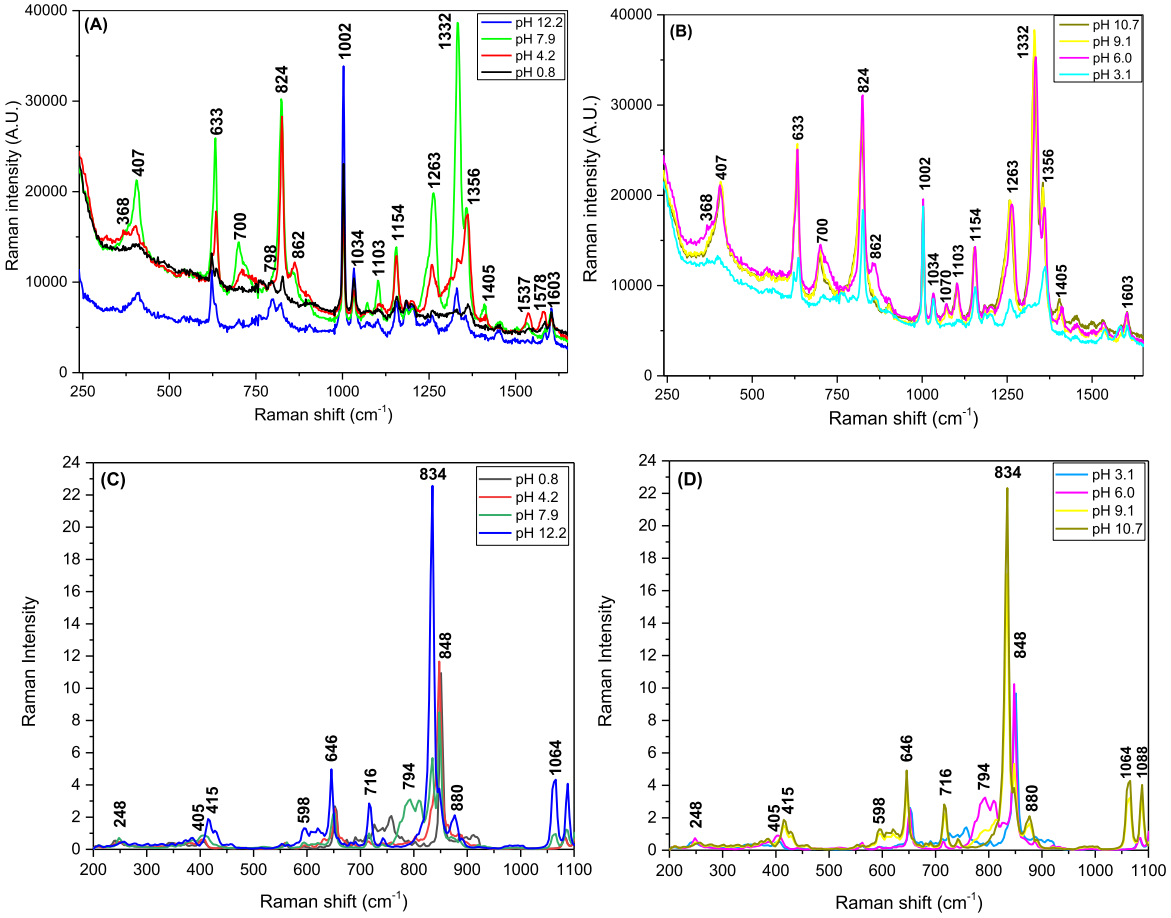

Fig. 3. Raman experimental (A, B) and computational (C, D) spectra of the roxarsone solutions at different pHs.

related to symmetric NO_2 stretching modes, while the doublet at 1537 and 1578 cm^{-1} corresponds to the $\nu_{as}(NO_2)$ stretching mode. The nitro group shows an electron-withdrawing effect on the aromatic ring, raising both the π character of the N=O bond and its Raman frequency [68]. Consequently, the Raman shifts of the NO_2 group also raise with the incorporation of electron-withdrawing groups to the benzene ring. Nonetheless, there are counterbalanced forces in the roxarsone case because the –OH group is in *ortho*-position and the arsonic group in *meta*-. The peak at 1002 cm^{-1} ascribes to the stretching modes of the Phe−OH group in roxarsone, suggesting the absence of an intramolecular hydrogen bond with the nitro group, which we can confirm by a visual inspection of our roxarsone clusters. Some examples of neutral roxarsone clusters were presented in Fig. S4, showing the absence of the intramolecular H-bond between the –OH of the Phe-OH group and the nitro group. This pattern appears in the roxarsone protomers found at another pH. Ring vibrations, including in-plane bending and aromatic ring vibrations, appeared particularly at 1033–1103 cm^{-1}. Such small shifts are associated with weak intermolecular bonding with other analyte molecules forming dimers or different complexes with water molecules.

Notwithstanding, the intensity of all these effects changes with pH, and consequently, different Raman peaks appear or disappear in the characteristic Raman shifts of the functional groups of the organoarsenicals with the pH variations (Table 3). In the theoretical spectra, the water molecules used as an explicit solvent in the simulations also emphasise the influence of the fluctuating solvent environment on the Raman activity and the frequencies of motions computed. As expected and observed in our previous study about the Raman spectra of arsenic oxoacids [38], the interaction with water molecules gives rise to a more significant number of theoretical Raman peaks in the frequency range studied, thus, making the peaks transform to bands because the water molecules effect.

Differences found between the Raman spectra of the different species of each organoarsenicals with pH are related to the changes suffered according to their acid-base behaviour. Arsanilic acids show an acid-base behaviour comparable to carboxylic acids. Thus, the following spectroscopic considerations arise at various particular pH values that predominate only one species of organoarsenicals (Table 3). Table 3 shows the peaks evolving with pH and the most probable responsible functional group. Some relationships exist between a few peaks and the corresponding pK_a values of the organoarsenicals. Thus, at very acidic pHs, the peaks relate to the protonated functional groups, while under alkaline conditions, the functional groups are largely or entirely deprotonated.

Let us now compare the experimental and theoretical spectra in a closer inspection of each solute. For brevity, we use the terms exp and *theor* as acronyms of *experimental* and *theoretical*, respectively, when we directly compare. For *o*-arsanilic acid and at pH 11.6, the most deprotonated species show a slight and a substantial increase of the Raman peaks in the experimental spectra at 1166 cm^{-1} (predominantly $-\ddot{N}H_2$ involved in H-bond confirmed by the visualisation of our cluster models) and 829 cm^{-1} (As=O), respectively. In the theoretical calculations (see Fig. 1 C, D), the As=O motion appears under a wideband located between 793 and 834 cm^{-1}. The theoretical calculations allow assigning this band not only to As=O motions but also to As-O^- normal modes that are strongly coupled to the solvent by H-bonds. Other changes occur at pH 3.7, where protonated species exist, generating two Raman peaks at 857 (exp) vs 865 cm^{-1} (*theor*) (As=O···H) and 717 (exp) vs 721 cm^{-1} (*theor*) (As−OH). Similarly, under very acidic conditions, pH 0.9, only the most protonated species exist, generating new Raman peaks at 771

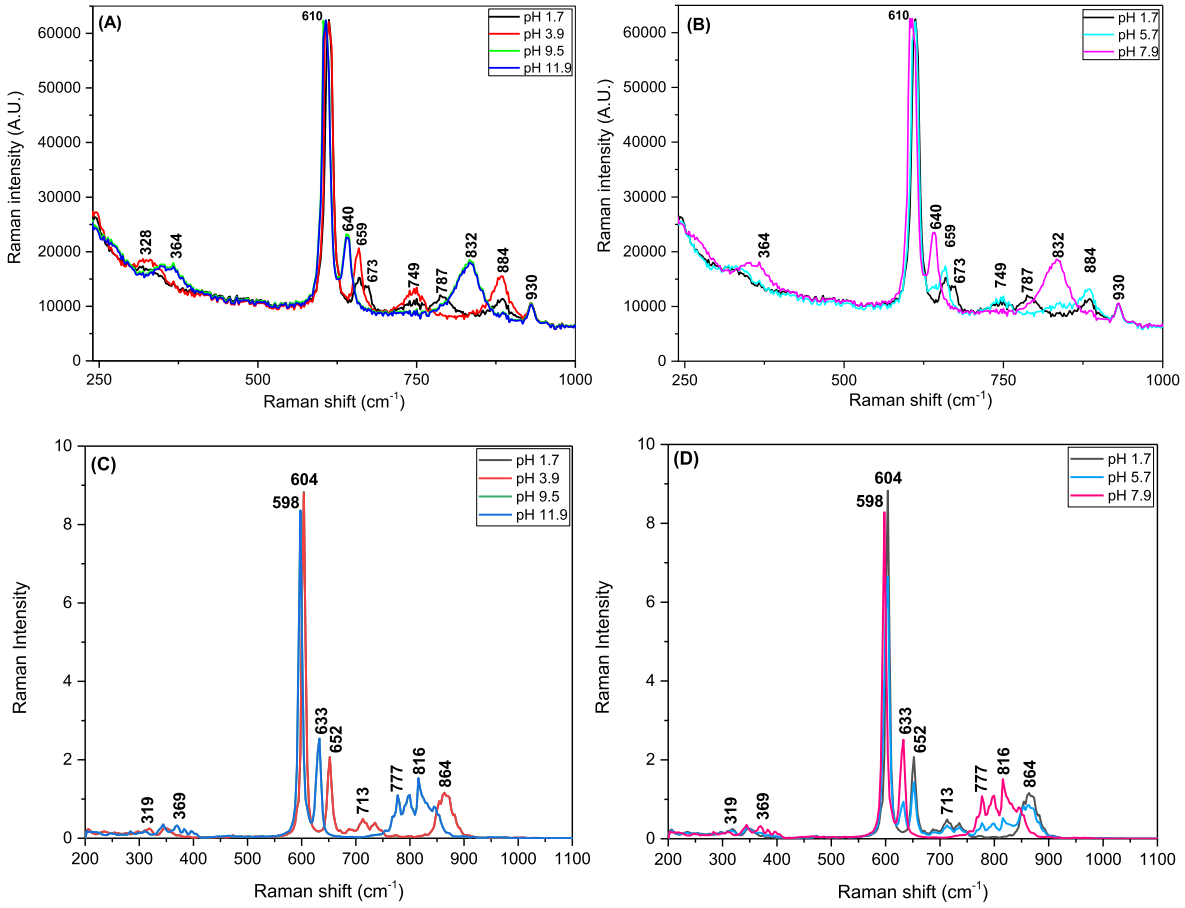

Fig. 4. Raman experimental (A, B) and computational (C, D) spectra of the cacodylic acid solutions at different pHs.

Table 1
Assignments of all experimental Raman bands of the organoarsenicals studied at any pH.

Assignments	Raman shifts, cm^{-1}			
	o-Arsanilic	*p*-Arsanilic	Roxarsone	Cacodylic acid
$\delta(AsO_2)$, $\rho(AsC_2)$				**328**
Wagging O=AsO$^-$	**386**	**397**		**364**
γ(CC); CN str.			**407**	
Out of plane ring def	**455**			
As-OH$_{(out\text{-}of\text{-}plane\ bending)}$	**555**			
As-C		**616,637**	**633**	**610,640**
ν_s(AsO)	**662**			**659, 673**
ν_s(As–OH)	**717**	**715**	**700**	**749**
ν_{as}(As–OH)	**771**	**763**		**787**
ν_s,ν_{as}(As=O)	**816, 829**	**818, 829**	**824**	**832**
ν_{as}(As=O…H)	**857**	**860**	**862**	**884**
$\nu_{as}(AsO_2)$, Rocking CH_3	**932**	**930**		**930**
Phe-OH			1002	
ν(CC)(Aromatic Ring)	1033	1100	1034, 1103	
ν(CN) + δ_{as}(CH) + $\delta_{as}(NH_2)$	1166, 1174	1187	1154	
ν(CN)	1211, **1247**	1216	**1263**	
$\nu_s(NH_2)$	**1311**	**1279**		
$\nu_s(NO_2)$			**1332, 1356**	
ν(CC) + δ_a(CH)	1405	1453	1405↓	
$\nu_{as}(NO_2)$ + C-C str			**1537**	
$\nu_{as}(NO_2)$			**1578**	
ν(CC)(Aromatic Ring)	1598	1600	1603	

(exp) vs. 768 cm^{-1} (*theor*) (As-OH), 816 (exp) vs. 820 cm^{-1} (*theor*) (As=O) and 1211 cm^{-1} (exp) (As-OH) increasing the intensity strongly at 932 cm^{-1} (As(=O)–$(OH)_2$), also suffering a red shifting from 829 to 816 cm^{-1} at pH 0.9. We also observe this shifting in the theoretical spectra from 834 to 820 cm^{-1}. Several peaks (771, 816, 932 and 1211 cm^{-1}) only appear under very acidic conditions (pH 0.9) with a similar pattern in the theoretical calculations. However, the Raman shifts observed in the experimental spectra at 717 and 857 cm^{-1} only exists in the pH range between 2.7 and 8.2, whilst in the theoretical calculations, this is not a very clear result. The peak at 386 cm^{-1} appears under alkaline conditions in both experimental and theoretical spectra and, finally, the strong Raman activity peak located at 1030–1033 cm^{-1} in both spectra is observed at any pH because it is unambiguously associated with the symmetrical stretching of the C–C bonds of the aromatic ring.

According to the pH value, the main Raman peaks noted for *p*-arsanilic acid are in Table 3. Thus, at pH 11.7, the experimental peak at 715 cm^{-1} (As-OH) disappears, and no evidence of this motion around this frequency appears in the theoretical spectra. We note in passing that the peak at 818 (exp) vs 820 cm^{-1} (*theor*) (As=O) emerges strongly. At pH 7.0, several intense peaks at 397 (exp) vs. 406 cm^{-1} (*theor*) and 616 (exp) vs. 614 cm^{-1} (*theor*) appear in the Raman spectra with a good concordance. However, at pH 7.0, the peak at 715 cm^{-1} related to As-OH motion appears, while this change is still absent in the theoretical calculations. By contrast, the overlapping of the 829 (As=O) and 860sh cm^{-1} coincides with a wide band around 844 cm^{-1} in the theoretical calculations. The wider band of the experimental spectra can be explained by the strong coupling of the solute motions with the H-bond water molecules, as shown in Fig. S3. As we observed in our previous work about arsenic oxoacid spectra [38], we confirm that the number of

Table 2
The most probable organoarsenicals species in solution at the pH values stated in the row below each one. We also included some hydrogen bonds for *o*-arsanilic acid and roxarsone.

Analyte	As species			
o-Arsanilic acid	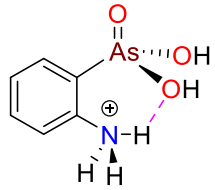	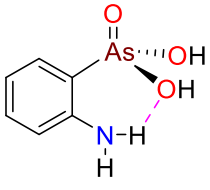	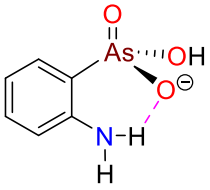	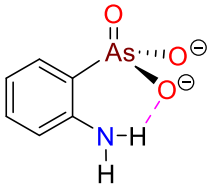
pH	**<1**	**2**	**3**	**>9**
p-Arsanilic acid	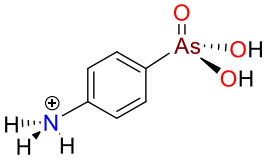	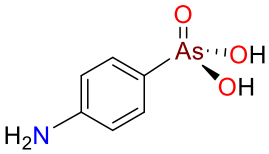	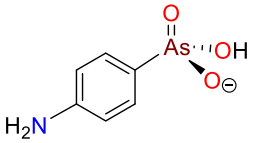	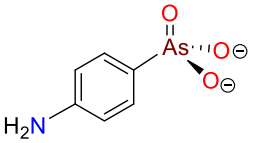
pH	**<1**	**3.2**	**6.5**	**>12**
Roxarsone	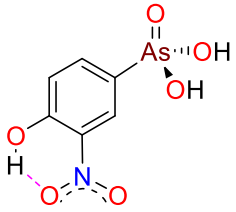	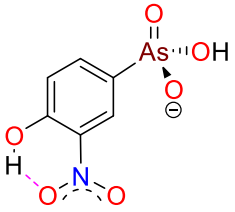	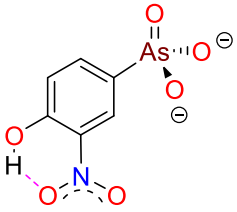	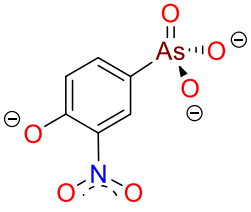
pH	**<1**	**5**	**8**	**>12**
Cacodylic acid	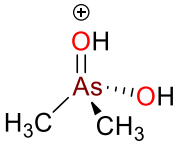		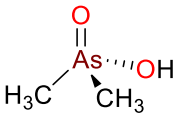	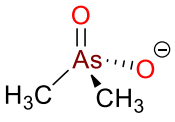
pH	**<1**		**4**	**>9**

water molecules is directly associated with the shape of the bands, making peaks wider and smaller. Note, however, that the theoretical spectra derive from models including only a few water molecules for computational reasons. At pH 7.0, the motion observed at 1600 cm^{-1} (aromatic ring) also appears in the Raman spectra. However, at pH 3.5, the peak at 830 cm^{-1} disappears in both experimental and theoretical spectra, while the peaks at 1553 cm^{-1} (aromatic ring) and 930 (exp) vs 915 cm^{-1} (*theor*) (As−O_x) increase stronger in experimental data. Similarly, at pH 0.1, the peaks at 397 (exp) vs. 406 cm^{-1} (*theor*), 616 (exp) vs. 614 cm^{-1} (*theor*) and 1600 cm^{-1} (exp) strongly decreased, while the peaks at 763 (exp) vs. 745 cm^{-1} (*theor*) (As-OH), 825 (exp) vs 832 cm^{-1} (*theor*) (As=O) and 1187 cm^{-1} (exp*)* grown. The peak at 397 (exp) vs 410 cm^{-1} (*theor*) appears in the pH range (4–12), where the zwitterionic form predominates. Notwithstanding the general agreement between the experimental and theoretical spectra, the wagging motion of the –NH_2 group at 450 cm^{-1} appears at pH 4.0–9.0 only in the theoretical spectra. It is possible to hypothesise that this result is due to the H-bond formation between the –NH_2 group and the water molecules in the experimental conditions. As explained in the methodology, for computational reasons, we only used a few numbers of water molecules around the arsonic/arsinic group because of our interest in identifying the motions related to As atoms. A closer inspection also shows other peaks at 715 (exp) vs. 732 cm^{-1} (*theor*) and 829 (exp) vs. 844 cm^{-1} (*theor*) that exist between pH 5.1 and pH 7.0, while others under acidic conditions (763 and 1216 cm^{-1} at pH 0.1, and 930 (exp) vs. 915 cm^{-1} (*theor*) at pH 1.8–3.5) and basic conditions (818 (exp) vs. a wider band between 800 and 830 cm^{-1} (*theor*) at pH 8.9 and 1279 (exp) cm^{-1} at pHs > 7.0). A more specific analysis shows that the wider band observed at 800–830 cm^{-1} in theoretical calculations correlates with the strong H-bond between the anionic protomer of *p*-arsanilic acid and the solvent water molecules. Finally, at pH > 8.9, the theoretical spectra present two peaks at 511 and 562 cm^{-1} related to the symmetrical and asymmetrical stretching of the C–C bonds of the aromatic ring. In the experimental spectra, these peaks are absent. It is possible to hypothesise that this finding comes from the H-bonds formed, on the one hand, between the –NH_2 group and the water molecules of the solvent and, on the other hand, between the deprotonated arsonic group and the water molecules which generate a clamp that blocks the possibility of the stretching motions of the aromatic ring significantly.

For roxarsone, the peaks at 407 (–CN), 633 (As=O), 700 (As−OH), 824, 1263 (As−OH), 1332 (–NO_2) and 1356 (–NO_2) cm^{-1} grown enormously from acidic pHs (0.8 – 4.2) to alkaline solutions (pH 7.9), decreasing again up to pH 12.2. We find a similar pattern to the previous one in the theoretical spectra. Due to the frequency range limitations, we noted the following motions in the theoretical spectra: 415 (–CN), 646 (As = O), 716 (As−OH) and 834 cm^{-1}. In a closer inspection of our cluster model, we can unambiguously assign the peak at 834 cm^{-1} to the strong scissoring of –NO_2 group simultaneously to the C-OH symmetrical stretching. Ongoing from acidic to basic conditions, we note in passing that this peak is broader and more likely a band due to the H-bond that the anionic roxarsone presents with the water molecules of the solvent. Contrarily, other peaks grow or decrease from alkaline to neutral and acidic solutions. It is worth remarking that the 1332/1356 ratio in the experimental spectra takes values < 0.5 and > 2.0 for pHs below 5.0 and above 6.0, respectively. Protonation of the nitro group under very acidic conditions would be behind the changes of this intensity ratio. This

Table 3
pH range of maximum existence for several experimental Raman peaks of the four organoarsenicals studied.

	Peaks, cm^{-1}	Most probable functional group	Existence pH
o-Arsanilic acid	386	O=As−O$^-$	11.6
	717	-As−OH	2.7 ↔ 8.7
	771	-As−$(OH)_2$	0.9
	816	-As=O	0.9
	829	-As=O	> 8.7
	857	-As=O···H	2.7 ↔ 8.7
	932	-AsO_2	0.9
	1211	C-N stretching	0.9
p-Arsanilic acid	397	O=As−O$^-$ (Zwiteronic form)	4.0 ↔ 12.0
	715	As−OH	5.1 ↔ 7.0
	763	As−OH	0.1
	818	As=O	8.9
	829	As=O	5.1 ↔ 7.0
	930	AsO_2	1.8 ↔ 3.5
	1216	C-N stretching	0.1
	1279	–NH_2	>7.0
Roxarsone	407	C−N, C-C	6.0 ↔ 10.7
	700	As−OH	6.0 ↔ 10.7
	824	As=O	4.2 ↔ 10.7
	862	As=O···H	4.2 ↔ 7.9
	1263	C-N	3.1 ↔ 10.7
	1332	NO_2	4 ↔ 12.2
	1356	NO_2	0.1 ↔ 12.2
	1537	NO_2	7.9
	1578	NO_2	12.2
Cacodylic acid	328	AsO_2	0.0 ↔ 6.0
	364	O=As−O$^-$	7.9 ↔ 11.9
	640	C-As	7.9 ↔ 11.9
	659	As=O···H	1.7 ↔ 5.7
	673	As=O	1.7
	749	As−OH	1.7 ↔ 5.7
	787	As−OH	1.7
	832	As=O	7.9 ↔ 11.9
	884	As=O···H	1.7 ↔ 5.7

intensity ratio grows from pH 12.2 to neutral conditions (pH 7.9) while it decreases again, lowering the pH. Structural differences of the nitro group as a function of pH are established in Table 3 [69]. The nitro group protonates asymmetrically one of the two oxygen where one N − O bond increases its bond order, whilst the other simultaneously decreases. Several changing peaks appear at 407 (exp) vs. 415 cm^{-1} (*theor*) and 700 (exp) vs. 716 cm^{-1} (*theor*) (pHs 6.0–10.7 (exp) vs. 6.0–12.2 (*theor*)), 824 (exp) vs. 834 cm^{-1} (*theor*) (pHs 4.2–10.7 (exp) vs. 7.9–12.2 (*theor*)) and 862 (exp) vs. 880 cm^{-1} (*theor*) (4.2–7.9 (exp) vs. 4.2–12.2 (*theor*)) with the predominance existence in the pH range stated into bracket. The As species responsible are also in Table 3. When comparing the experimental and theoretical spectra, a remarkable peak appeared at 848 cm^{-1}. Its Raman activity decreases from acidic to basic conditions, and it presents a special low Raman activity at pH > 10.7. Our cluster models allow assigning this vibration mode to multiple motions related to scissoring of the –NO_2 group, rocking of the Phe-OH group and symmetrical stretching of the C–C bonds in the aromatic ring. As observed for *p*-arsenic acid, these peaks are absent. Once again, it is possible to hypothesise that the H-bonds formed between these groups and the deprotonated arsonic group with the water molecules solvent favours a clamp formation that blocks the related motions. Finally, the 1034 (exp) vs 1064 cm^{-1} (*theor*) peak, observed in both spectra, is related to the C–C motion in the aromatic ring.

Cacodylic acid is quite different because it does not support an aromatic ring in its structure. Nonetheless, under alkaline conditions, pHs 9.5 and 11.9, the deprotonated form predominates, showing the Raman peaks at 364 (exp) vs. 369 cm^{-1} (*theor*) (As(=O)−O$^-$), 640 (exp) vs. 633 cm^{-1} (*theor*) (As→O$^{\delta-}$), 832 (exp) vs. 816 cm^{-1} (*theor*) (As = O), and 930 (exp) (As=O), while under acidic conditions, pH < 3.9, we noted the new peaks at 328 (exp) vs. 319 cm^{-1} (*theor*), 659 (exp) vs. 652 cm^{-1} (*theor*) (As=O···H···), 749 (exp) vs. 750–777 cm^{-1} (*theor*) (As−OH) and 884 (exp) vs. 834 cm^{-1} (*theor*) (As=O···H). Two peaks suffer a bathochromic shift decreasing pH. Thus, the experimental peak at 832 cm^{-1} shifts to 884 cm^{-1} from alkaline to neutral solutions, whilst the theoretical calculations report this shift to be from 816 to 864 cm^{-1}. Similarly, the peak at 640 cm^{-1} shifts to 659 cm^{-1} and then to 673 cm^{-1} from alkaline to neutral and acidic pHs, whilst these differences appear at 633 → 652 cm^{-1} in the theoretical spectra. The small peak at 364 (exp) vs 369 cm^{-1} (*theor*) decreases, lowering the pH. This behaviour relates to the protonation/deprotonation processes of the As−O···H group of the arsinic acid and the conclusive formation of dimers (self-association) [67]. In our cluster models, we confirmed the existence of a higher number of H-bonds (of the type As-O$^{(anionic)}$···H) than those found in acidic conditions, where the interactions between As-O···H and As-OH···H are predominant but with less relevance. However, under very acidic conditions, pH 1.7, two new experimental peaks evolve at 673 (As−O···H$^{\delta+}$) and 787 cm^{-1} (As−OH), ascribed to the ammonium group. We do not note these motions in our cluster models since we used a few numbers of water molecules (~6–8) to reproduce the environment of the arsinic group. It is worth remarking that the Raman peak at 607 (exp) vs 598–604 cm^{-1} (*theor*) remains constant at any pH, which offers an exciting opportunity to detect the presence of cacodylic acid in aqueous solutions under any pH conditions. In a finer inspection, we assigned this frequency mode to the symmetrical stretching of CH_3-As in the cacodylic acid. The inexistence of H-bonds or protonation/deprotonation of As atom and –CH_3 groups makes this motion found at any pH. Several changing peaks also exist at pH 1.7 (673, 787 cm^{-1}), pH 0.0–6.0 (328 cm^{-1}), pHs 1.7–5.7 (659, 749 and 884 cm^{-1}), and pHs 7.9–11.9 (364, 640 and 832 cm^{-1}) (Table 3). Similar to that reported in the experimental spectra, a frequency pattern appeared with slight deviations in the theoretical spectra. We note in passing that at pH > 7.9, the experimental band at 787–884 cm^{-1} can be found in a very agreement at 777–860 cm^{-1} in theoretical simulations. Looking at our cluster models, this band unambiguously assigns to the strong H-bonds formed between the anionic arsinic group and the water molecules of the solvent. The Raman spectra obtained at some intermediate pHs show overlapped peaks from the two organoarsenicals species involved, depending on the pH selected (Figs. 1-4 B, Fig. S6). Further, the Raman experimental and theoretical bands noted represent some logical slightly shifting and broadening, according to the predominance of each organoarsenic species (Figs. 1-4). One of the advantages of the computational calculations of Raman spectra is identifying each vibration mode and assessing the contribution of the water molecules of solvent on it. For the sake of completion and for comparison with the arsenic oxoacids Raman spectra previously studied [38], we evaluated the H_2O weight in motion in each vibration mode found in theoretical calculations of cacodylic acid (see Table S2). This evaluation shows an overall water influence in motions of 25% in the neutral cacodylic acid against 32% in the anionic cacodylic acid protomer. This water coupling was similar to that found in the tetrahedral H_3AsO_4 (~23%) but lower than other As oxoacids (*e.g.* $H_2AsO_4^-$ (48%); H_3AsO_3 (49%)). The more hydrophobicity of the –CH_3 groups presented in the cacodylic acid and its conjugate base is probable behind this trend. Similar information and conclusions can be achieved for other organoarsenicals.

The bending vibrations of As–OH at 1272 and 555 cm^{-1} and As–O at 865 cm^{-1} do not appear in the Raman spectra of arsanilic acid, which involves forming self-associations and open chains through intermolecular hydrogen bonds but also cyclic structures as a result of the intramolecular hydrogen bonding (see Fig. S2) [70,71]. However, the Raman bands at 2934 and 3064 cm^{-1}, related to hydroxyl stretching vibrations, suggesting hydrogen bonds (–OH···O-) (Fig. S7), particularly for cacodylic acid, which involve water molecules and the oxygen of the arsinic group [72], what is notably evident for solid phases [73].

3.3. Analytical implications

Organoarsenicals include toxic and non-toxic compounds, and their speciation is essential for adequate legislation to establish regulatory limits in different matrices for this type of compound. It is usual to achieve quantitative data using complex sample preparation procedures and sophisticated analytical techniques [74]. Nonetheless, a permanent goal of Analytical Chemistry is to simplify all stages of the analytical procedure. In this way, the possibility to incorporate direct analyses is a challenge.

According to the results found in the above sections, we can follow several qualitative and quantitative analytical possibilities depending on the organoarsenicals involved and pH conditions. Thus, a few Raman shifts are characteristic for each organoarsenicals species stated at different pH values (Table 3). Remarkably, the Raman peaks 771, 816, 1211 cm^{-1} allow us to characterise *o*-arsanilic at a very acidic pH (0.9); the peak at 857 cm^{-1} always appears in the pH range between 2.7 and 10.0; while the peak at 829 cm^{-1} grows for pHs above 8.0. Something similar occurs for the *p*-arsanilic acid, which shows specific Raman peaks at 763 and 715 cm^{-1} at very acidic pH (0.1) and neutral pH (7.0), respectively, while the peak at 1600 cm^{-1} grows from pH 0.0 to 8.0. For the other organoarsenicals included in this work, we found similar considerations. Thus, the peaks 633 and 1263 cm^{-1} in the Raman spectra of roxarsone grow from pH 0.0 to 8.0, whilst the ratio of the peaks, 1332/1356, grows with pH, indicating the presence of roxarsone. Diverse Raman peaks also characterise cacodylic acid at different pHs. The peaks at 787 and 673 cm^{-1} are typical at pH 1.0; 659 cm^{-1} at pH 4.0 ↔ 6.0, and 832 and 640 cm^{-1} at pHs between 7.0 and 12.0. Each of these peaks allows us an easy qualitative identification of the corresponding organoarsenicals species as a function of pH.

For mixtures of the four organoarsenicals, differentiation between them is possible to reference the following Raman peaks. Thus, at pH 12.0, the peaks at 555, 663, 1033 and 1165 cm^{-1} are characteristic of *o*-arsanilic acid, while the small peak at 610 cm^{-1} and the increased peak at 639 cm^{-1} confirm the presence of *p*-arsanilic acid. Similarly, an intense peak at 608 cm^{-1} and another small one at 640 cm^{-1} is helpful to characterise the presence of roxarsone, whilst an increased peak at 1003 cm^{-1} in combination with another small one at 1035 cm^{-1} is an indication of the presence of cacodylic acid. At neutral pHs, the most characteristic feature is the pattern of peaks constituted by 633, 700, 1002, 1154, 1236, 1332, 1356 cm^{-1}found for roxarsone.

Furthermore, we found several linear relationships between the analyte concentration (x) and Raman intensity (y) of some peaks. Thus, the following straight-line equation $y = (1700 \pm 500) + (89600 \pm 1600)x$ ($R^2 = 0.99935$) exists in the concentration range between 1 M and 3 M and the pH 0.5–10.0 range for cacodylic acid using the 606 cm^{-1} Raman shift. Similarly, for *p*-arsanilic and *o*-arsanilic acids in the same concentration range, 1 M−3 M, the straight lines $y = (75 \pm 70) + (52700 \pm 200)x$ ($R^2 = 0.99996$) and $y = (-160 \pm 150) + (36500 \pm 500)x$ ($R^2 = 0.99966$) were found at pHs 7.0 and 8.2, respectively, and the wavenumbers 1100 and 662 cm^{-1} for the corresponding analyte (Table 1). With the wavenumbers evaluated, we achieved an excellent repeteability in the quantitation of the analytes varying between 0.004 M and 0.010 M for all analytes under the pH conditions stated through the text.

4. Conclusions

The structural elucidation of organoarsenicals compounds in aqueous solution at different pHs was possible by Raman spectrometry. Direct analysis of the sample is an additional advantage making this procedure very attractive for environmental monitoring. Unequivocal speciation is possible since each compound possesses unique spectral features depending on the solution pH. The peaks ascribed to amino (–NH_2), nitro (–NO_2), hydroxyl (–OH), but mainly to arsonic (R−As(=O)−$(OH)_2$) and arsinic (R−As(=O)−(OH)) groups were essential in the identification of the corresponding compounds.

Despite the presence of charged species, the most remarkable feature is that conventional DFT calculations reasonably reproduced the organoarsenicals spectra in an aqueous solution, providing the models involve explicit solvent molecules and some conformational averages. Some differences between theory and experiment arise in the positioning and relative intensity of the more critical peaks and the appearance of other low-intensity bands. Considering the significant coupling between the organoarsenicals and water molecules, more accurate predictions would require the inclusion of other explicit water molecules, incorporating more specific scale factors and accounting for anharmonicity effects. No differences exist in the fitting when compared aromatic versus aliphatic organoarsenicals.

CRediT authorship contribution statement

R. López: Methodology, Writing – review & editing, Supervision. **F. J. Pereira:** Methodology, Writing – review & editing, Supervision. **D. Suárez:** Conceptualization, Methodology, Writing – review & editing. **A. J. Aller:** Conceptualization, Methodology, Writing – review & editing.

Declaration of Competing Interest

The authors declare that they have no known competing financial interests or personal relationships that could have appeared to influence the work reported in this paper.

Acknowledgement

We acknowledge support from the PGC2018-095953-B grant (MICINN, Spain). This research did not receive any specific grant from funding agencies in the commercial or not-for-profit sectors.

Appendix A. Supplementary data

Supplementary data to this article can be found online at https://doi.org/10.1016/j.microc.2022.107186.

References

[1] J. Lu, E.-H. Chew, A. Holmgren, Targeting thioredoxin reductase is a basis for cancer therapy by arsenic trioxide, Proc. Natl. Acad. Sci. USA 104 (30) (2007) 12288–12293, https://doi.org/10.1073/pnas.0701549104.
[2] N.C. Lloyd, H.W. Morgan, B.K. Nicholson, R.S. Ronimus, The composition of Ehrlich's Salvarsan: resolution of a century-old debate, Angew. Chemie - Int. Ed. 44 (6) (2005) 941–944, https://doi.org/10.1002/anie.200461471.
[3] N.C. Lloyd, H.W. Morgan, B.K. Nicholson, R.S. Ronimus, Substituted phenylarsonic acids; structures and spectroscopy, J. Organomet. Chem. 693 (14) (2008) 2443–2450, https://doi.org/10.1016/j.jorganchem.2008.04.033.
[4] S.V. Barrett, M.P. Barrett, Anti-sleeping sickness drugs and cancer chemotherapy, Parasitol. Today 16 (1) (2000) 7–9, https://doi.org/10.1016/S0169-4758(99)01560-4.
[5] S. Waxman, K.C. Anderson, History of the development of arsenic derivatives in cancer therapy, Oncologist 6 (2001) 3–10, https://doi.org/10.1634/theoncologist.6-suppl_2-3.
[6] W.H. Miller, H.M. Schipper, J.S. Lee, J. Singer, S. Waxman, Mechanisms of action of arsenic trioxide - Universidad de León - Biblioteca, Cancer Res. 62 (2002) 3893–3903.
[7] H. Chen, R.C. MacDonald, S. Li, N.L. Krett, S.T. Rosen, T.V. O'Halloran, Lipid encapsulation of arsenic trioxide attenuates cytotoxicity and allows for controlled anticancer drug release, J. Am. Chem. Soc. 128 (41) (2006) 13348–13349, https://doi.org/10.1021/ja064864h.
[8] Y. Nakamura, T. Narukawa, J. Yoshinaga, Cancer risk to Japanese population from the consumption of inorganic arsenic in cooked hijiki, J. Agric. Food Chem. 56 (7) (2008) 2536–2540, https://doi.org/10.1021/jf0731797.
[9] R.L. Zimdahl, Fundamentals of weed science, in: Fundamentals of Weed Science, Elsevier, 2018, pp. 651–681, https://doi.org/10.1016/B978-0-12-811143-7.00023-8.
[10] J.R. Garbarino, A.J. Bednar, D.W. Rutherford, R.S. Beyer, R.L. Wershaw, Environmental fate of roxarsone in poultry litter. I. Degradation of roxarsone during composting, Environ. Sci. Technol. 37 (8) (2003) 1509–1514, https://doi.org/10.1021/es026219q.
[11] R. Raml, W. Goessler, P. Traar, T. Ochi, K.A. Francesconi, Novel thioarsenic metabolites in human urine after ingestion of an arsenosugar, 2′,3′-

dihydroxypropyl 5-deoxy-5-dimethylarsinoyl- β-D-riboside, Chem. Res. Toxicol. 18 (2005) 1444–1450, https://doi.org/10.1021/tx050111h.
[12] J.G. Hering, S.J. Hug, C. Farnsworth, P.A. O'Day, Role of coupled redox transformations in the mobilization and sequestration of arsenic, in: ACS Symp. Ser., American Chemical Society, 2011: pp. 463–476. doi:10.1021/bk-2011-1071.ch021.
[13] I. Cortinas, J.A. Field, M. Kopplin, J.R. Garbarino, A.J. Gandolfi, R. Sierra-Alvarez, Anaerobic biotransformation of roxarsone and related N-substituted phenylarsonic acids, Environ. Sci. Technol. 40 (9) (2006) 2951–2957, https://doi.org/10.1021/es051981o.
[14] R. Bentley, T.G. Chasteen, Microbial methylation of metalloids: arsenic, antimony, and bismuth, Microbiol. Mol. Biol. Rev. 66 (2) (2002) 250–271.
[15] V.M. Dembitsky, T. Rezanka, Natural occurrence of arseno compounds in plants, lichens, fungi, algal species, and microorganisms, Plant Sci. 165 (6) (2003) 1177–1192, https://doi.org/10.1016/j.plantsci.2003.08.007.
[16] V.M. Dembitsky, D.O. Levitsky, Arsenolipids, Prog. Lipid Res. 43 (5) (2004) 403–448, https://doi.org/10.1016/j.plipres.2004.07.001.
[17] K.A. Francesconi, S. Khokiattiwong, W. Goessler, S.N. Pedersen, M. Pavkov, A new arsenobetaine from marine organisms identified by liquid chromatography-mass spectrometry, Chem. Commun. (2000) 1083–1084, https://doi.org/10.1039/b002392m.
[18] Y. Yamaoka, M.L. Carmona, J.M. Oclarit, K. Jin, Y. Shibata, Arsenic compounds in marine sponge (Haliclona permolis, Halichondria japonica, Halichondria okadai andHaliclona sp. white) from Seto Inland Sea, Japan, Appl. Organometal. Chem. 15 (4) (2001) 261–265.
[19] A. Rumpler, J. Edmonds, M. Katsu, K. Jensen, W. Goessler, G. Raber, H. Gunnlaugsdottir, K. Francesconi, Arsenic-containing long-chain fatty acids in cod-liver oil: a result of biosynthetic infidelity? Angew. Chem. 120 (14) (2008) 2705–2707, https://doi.org/10.1002/ange.200705405.
[20] A. Raab, S. Wright, M. Jaspars, A. Meharg, J. Feldmann, Pentavalent arsenic can bind to biomolecules, Angew. Chem. 119 (15) (2007) 2648–2651, https://doi.org/10.1002/ange.200604805.
[21] J.F. Stolz, E. Perera, B. Kilonzo, B. Kail, B. Crable, E. Fisher, M. Ranganathan, L. Wormer, P. Basu, Biotransformation of 3-nitro-4-hydroxybenzene arsonic acid (Roxarsone) and release of inorganic arsenic by clostridium species, Environ. Sci. Technol. 41 (3) (2007) 818–823, https://doi.org/10.1021/es061802i10.1021/es061802i.s001.
[22] B.P. Jackson, P.M. Bertsch, Determination of arsenic speciation in poultry wastes by IC-ICP-MS, Environ. Sci. Technol. 35 (24) (2001) 4868–4873, https://doi.org/10.1021/es0107172.
[23] A.R. Roerdink, J.H. Aldstadt, Sensitive method for the determination of roxarsone using solid-phase microextraction with multi-detector gas chromatography, J. Chromatogr. A. 1057 (1-2) (2004) 177–183, https://doi.org/10.1016/j.chroma.2004.09.071.
[24] C.G. Rosal, G.-M. Momplaisir, E.M. Heithmar, Roxarsone and transformation products in chicken manure: determination by capillary electrophoresis-inductively coupled plasma-mass spectrometry, Electrophoresis 26 (7-8) (2005) 1606–1614, https://doi.org/10.1002/elps.200406198.
[25] F.J. Pereira, M.D. Vázquez, L. Debán, A.J. Aller, Inorganic arsenic speciation by differential pulse anodic stripping voltammetry using thoria nanoparticles-carbon paste electrodes, Talanta 152 (2016) 211–218, https://doi.org/10.1016/j.talanta.2016.02.011.
[26] F.J. Pereira, M.D. Vázquez, L. Debán, A.J. Aller, Cyclic voltammetry of arsenic-doped cysteine-capped ceramic nanoparticles, Electrochim. Acta 109 (2013) 125–135, https://doi.org/10.1016/j.electacta.2013.07.087.
[27] A.F. Villadangos, E. Ordóñez, M.I. Muñoz, I.M. Pastrana, M. Fiuza, J.A. Gil, L. M. Mateos, A.J. Aller, Retention of arsenate using genetically modified coryneform bacteria and determination of arsenic in solid samples by ICP-MS, Talanta 80 (3) (2010) 1421–1427, https://doi.org/10.1016/j.talanta.2009.09.046.
[28] S. Cowen, M. Duggal, T. Hoang, H.A. Al-Abadleh, Vibrational spectroscopic characterization of some environmentally important organoarsenicals - A guide for understanding the nature of their surface complexes, Can. J. Chem. 86 (10) (2008) 942–950.
[29] K. Kneipp, H. Kneipp, I. Itzkan, R.R. Dasari, M.S. Feld, Ultrasensitive chemical analysis by Raman spectroscopy, Chem. Rev. 99 (10) (1999) 2957–2976, https://doi.org/10.1021/cr980133r.
[30] K. Kneipp, H. Kneipp, I. Itzkan, R.R. Dasari, M.S. Feld, Surface-enhanced Raman scattering and biophysics, J. Phys. Condens. Matter. 14 (2002) 597–624. https://iopscience.iop.org/article/10.1088/0953-8984/14/18/202/meta.
[31] M. Thomas, M. Brehm, R. Fligg, P. Vöhringer, B. Kirchner, Computing vibrational spectra from ab initio molecular dynamics, Phys. Chem. Chem. Phys. 15 (2013) 6608–6622, https://doi.org/10.1039/C3CP44302G.
[32] J.O. Jensen, S.J. Gilliam, A. Banerjee, D. Zeroka, S.J. Kirkby, C.N. Merrow, A theoretical study of As4O6: vibrational analysis, infrared and Raman spectra, J. Mol. Struct. THEOCHEM. 664–665 (2003) 145–156, https://doi.org/10.1016/j.theochem.2003.08.109.
[33] I. Dhouib, P. Guionneau, Z. Elaoud, Vibrational spectroscopy, electrical characterization, nonlinear optical properties and DFT calculation of (NEt4)(H2AsO4)(H3AsO4)2, J. Coord. Chem. 70 (21) (2017) 3585–3597, https://doi.org/10.1080/00958972.2017.1406082.
[34] M. Yang, Y. Sun, X. Zhang, B. McCord, A.J. McGoron, A. Mebel, Y. Cai, Raman spectra of thiolated arsenicals with biological importance, Talanta. 179 (2018) 520–530, https://doi.org/10.1016/j.talanta.2017.11.022.
[35] A.J. Karttunen, M. Linnolahti, T.A. Pakkanen, Icosahedral and ring-shaped allotropes of arsenic, ChemPhysChem. 8 (16) (2007) 2373–2378, https://doi.org/10.1002/cphc.200700376.
[36] P. Nava, R. Ahlrichs, Theoretical Investigation of clusters of phosphorus and arsenic: fascination and temptation of high symmetries chemistry-a European journal, Chem Eur. J. 14 (2008) 4039–4045.
[37] N. Ennaceur, R. Henchiri, B. Jalel, M. Cordier, I. Ledoux-Rak, E. Elaloui, Synthesis, crystal structure, and spectroscopic characterization supported by DFT calculations of organoarsenic compound, J. Mol. Struct. 1144 (2017) 25–32, https://doi.org/10.1016/j.molstruc.2017.05.007.
[38] F.J. Pereira, R. López, D. Suárez, A.J. Aller, pH-dependent structural changes of arsenic oxoacids in solution and solid phase: Raman spectrometry and computational studies, Microchem. J. 175 (2022) 107109, https://doi.org/10.1016/j.microc.2021.107109.
[39] A.D. Becke, Density-functional thermochemistry. III. The role of exact exchange, J. Chem. Phys. 98 (7) (1993) 5648–5652, https://doi.org/10.1063/1.464913.
[40] C. Lee, W. Yang, R.G. Parr, Development of the Colle-Salvetti correlation-energy formula into a functional of the electron density, Phys. Rev. B. 37 (2) (1988) 785–789, https://doi.org/10.1103/PhysRevB.37.785.
[41] T.H. Dunning, Gaussian basis sets for use in correlated molecular calculations. I. The atoms boron through neon and hydrogen, J. Chem. Phys. 90 (2) (1989) 1007–1023, https://doi.org/10.1063/1.456153.
[42] K.A. Peterson, T.H. Dunning, Accurate correlation consistent basis sets for molecular core-valence correlation effects: the second row atoms Al-Ar, and the first row atoms B-Ne revisited, J. Chem. Phys. 117 (23) (2002) 10548–10560, https://doi.org/10.1063/1.1520138.
[43] D.E. Woon, T.H. Dunning, Gaussian basis sets for use in correlated molecular calculations. V. Core-valence basis sets for boron through neon, J. Chem. Phys. 103 (11) (1995) 4572–4585, https://doi.org/10.1063/1.470645.
[44] M.K. Kesharwani, B. Brauer, J.M.L. Martin, Frequency and zero-point vibrational energy scale factors for double-hybrid density functionals (and other selected methods): can anharmonic force fields be avoided? J. Phys. Chem. A. 119 (2015) 1701–1714, https://doi.org/10.1021/JP508422U/SUPPL_FILE/JP508422U_SI_002.PDF.
[45] P. Sinha, S.E. Boesch, C. Gu, R.A. Wheeler, A.K. Wilson, Harmonic vibrational frequencies: scaling factors for HF, B3LYP, and MP2 methods in combination with correlation consistent basis sets, J. Phys. Chem. A. 108 (2004) 9213–9217, https://doi.org/10.1021/JP048233Q/SUPPL_FILE/JP048233QSI20040601_010714.PDF.
[46] G. Rauhut, P. Pulay, Transferable scaling factors for density functional derived vibrational force fields, J. Phys. Chem. 99 (1995) 3093–3100, https://doi.org/10.1021/J100010A019/SUPPL_FILE/JP3093.PDF.
[47] J. Tomasi, B. Mennucci, E. Cances, The IEF version of the PCM solvation method: an overview of a new method addressed to study molecular solutes at the QM ab initio level, J. Mol. Struct. THEOCHEM. 464 (1999) 211–226.
[48] C.S. Pomelli, J. Tomasi, V. Barone, An improved iterative solution to solve the electrostatic problem in the polarizable continuum model, Theor. Chem. Acc. 105 (6) (2001) 446–451.
[49] M.J. Frisch, G.W. Trucks, H.B. Schlegel, G.E. Scuseria, M.A. Robb, J.R. Cheeseman, G. Scalmani, V. Barone, G.A. Petersson, H. Nakatsuji, X. Li, M. Caricato, A. V Marenich, J. Bloino, B.G. Janesko, R. Gomperts, B. Mennucci, H.P. Hratchian, J. V Ortiz, A.F. Izmaylov, J.L. Sonnenberg, D. Williams-Young, F. Ding, F. Lipparini, F. Egidi, J. Goings, B. Peng, A. Petrone, T. Henderson, D. Ranasinghe, V.G. Zakrzewski, J. Gao, N. Rega, G. Zheng, W. Liang, M. Hada, M. Ehara, K. Toyota, R. Fukuda, J. Hasegawa, M. Ishida, T. Nakajima, Y. Honda, O. Kitao, H. Nakai, T. Vreven, K. Throssell, J.J.A. Montgomery, J.E. Peralta, F. Ogliaro, M.J. Bearpark, J. J. Heyd, E.N. Brothers, K.N. Kudin, V.N. Staroverov, T.A. Keith, R. Kobayashi, J. Normand, K. Raghavachari, A.P. Rendell, J.C. Burant, S.S. Iyengar, J. Tomasi, M. Cossi, J.M. Millam, M. Klene, C. Adamo, R. Cammi, J.W. Ochterski, R.L. Martin, K. Morokuma, O. Farkas, J.B. Foresman, D.J. Fox, Gaussian 16, Revision C.01, Gaussian, Inc.,. (2016).
[50] S. Grimme, A. Hansen, J.G. Brandenburg, C. Bannwarth, Dispersion-corrected mean-field electronic structure methods, Chem. Rev. 116 (9) (2016) 5105–5154, https://doi.org/10.1021/acs.chemrev.5b00533.
[51] S. Grimme, J. Antony, S. Ehrlich, H. Krieg, A consistent and accurate ab initio parametrization of density functional dispersion correction (DFT-D) for the 94 elements H-Pu, J. Chem. Phys. 132 (15) (2010) 154104, https://doi.org/10.1063/1.3382344.
[52] S. Corni, C. Cappelli, R. Cammi, J. Tomasi, Theoretical approach to the calculation of vibrational Raman spectra in solution within the polarizable continuum model, J. Phys. Chem. A. 105 (36) (2001) 8310–8316, https://doi.org/10.1021/jp011079c.
[53] G. Caballero-García, G. Mondragón-Solórzano, R. Torres-Cadena, M. Díaz-García, J. Sandoval-Lira, J. Barroso-Flores, Calculation of VS, max and its use as a descriptor for the theoretical calculation of pKa values for carboxylic acids, Molecules. 24 (2018) 79, https://doi.org/10.3390/MOLECULES24010079.
[54] S. Liu, L.G. Pedersen, Estimation of molecular acidity via electrostatic potential at the nucleus and valence natural atomic orbitals, J. Phys. Chem. A. 113 (15) (2009) 3648–3655.
[55] A. Martín Pendás, E. Francisco, Real space bond orders are energetic descriptors, Phys. Chem. Chem. Phys. 20 (23) (2018) 16231–16237, https://doi.org/10.1039/C8CP02485E.
[56] A.M. Pendás, E. Francisco, PROMOLDEN: A QTAIM/IQA code, Unpublished. (2015).
[57] W.L. Jorgensen, J. Chandrasekhar, J.D. Madura, R.W. Impey, M.L. Klein, Comparison of simple potential functions for simulating liquid water, J. Chem. Phys. 79 (2) (1983) 926–935.
[58] R. Salomon-Ferrer, D.A. Case, R.C. Walker, An overview of the Amber biomolecular simulation package, Wiley Interdiscip. Rev. Comput. Mol. Sci. 3 (2) (2013) 198–210, https://doi.org/10.1002/wcms.1121.

[59] I.Y.B.-S. D.A. Case S.R. Brozell, D.S. Cerutti, T.E. Cheatham, III, V.W.D. Cruzeiro, T. A. Darden, R.E. Duke, D. Ghoreishi, M.K. Gilson, H. Gohlke, A.W. Goetz, D. Greene, R Harris, N. Homeyer, S. Izadi, A. Kovalenko, T. Kurtzman, T.S. Lee, S. LeGrand, P. Li, C. Lin, AMBER 2018, (2018).
[60] A.K. Rappé, C.J. Casewit, K.S. Colwell, W.A. Goddard, W.M. Skiff, UFF, a full periodic table force field for molecular mechanics and molecular dynamics simulations, J. Am. Chem. Soc. 114 (1992) 10024–10035, https://doi.org/10.1021/JA00051A040/SUPPL_FILE/JA00051A040_SI_001.PDF.
[61] T. Lu, F. Chen, Multiwfn: a multifunctional wavefunction analyzer, J. Comput. Chem. 33 (5) (2012) 580–592, https://doi.org/10.1002/jcc.22885.
[62] K.S. Pitzer, Activity Coefficients in Electrolyte Solutions, 2nd ed., Florida, USA, Boca Raton, 1991.
[63] H. Yang, Q. Wang, Q. Zhou, J. Yue, Isopiestic measurements of water activities for an arsenic acid aqueous solution at 298.15 K, J. Chem. Eng. Data. 62 (10) (2017) 3306–3312, https://doi.org/10.1021/acs.jced.7b00349.
[64] F.J. Millero, The estimation of the pKHA of acids in seawater using the Pitzer equations, Geochim. Cosmochim. Acta 47 (12) (1983) 2121–2129, https://doi.org/10.1016/0016-7037(83)90037-6.
[65] M.C. Simoes, K.J. Hughes, D.B. Ingham, L. Ma, M. Pourkashanian, Estimation of the pitzer parameters for 1–1, 2–1, 3–1, 4–1, and 2–2 single electrolytes at 25 °c, J. Chem. Eng. Data 61 (7) (2016) 2536–2554, https://doi.org/10.1021/acs.jced.6b00236.
[66] P.M. May, D. Rowland, Thermodynamic modeling of aqueous electrolyte systems: current status, J. Chem. Eng. Data. 62 (9) (2017) 2481–2495, https://doi.org/10.1021/acs.jced.6b01055.
[67] V.V. Mulloyarova, A.M. Puzyk, A.A. Efimova, A.S. Antonov, R.A. Evarestov, I. S. Aliyarova, R.E. Asfin, P.M. Tolstoy, Solid-state and solution-state self-association of dimethylarsinic acid: IR, NMR and theoretical study, J. Mol. Struct. 1234 (2021) 130176.
[68] C. Passingham, P.J. Hendra, C. Hodges, H.A. Willis, The Raman spectra of some aromatic nitro compounds, Spectrochim. Acta Part A Mol. Spectrosc. 47 (9-10) (1991) 1235–1245, https://doi.org/10.1016/0584-8539(91)80210-A.
[69] O. Exner, S. Böhm, Protonated nitro group: structure, energy and conjugation, Org. Biomol. Chem. 3 (2005) 1838–1843, https://doi.org/10.1039/B502152A.
[70] B.A. Kolesov, Hydrogen bonds: Raman spectroscopic study, Int. J. Mol. Sci. 22 (2021) 5380, https://doi.org/10.3390/IJMS22105380.
[71] A.D. Buckingham, J.E. Del Bene, S.A.C. McDowell, The hydrogen bond, Chem. Phys. Lett. 463 (1-3) (2008) 1–10.
[72] M.A. Gomez, H. Assaaoudi, L. Becze, J.N. Cutler, G.P. Demopoulos, Vibrational spectroscopy study of hydrothermally produced scorodite (FeAsO4·2H2O), ferric arsenate sub-hydrate (FAsH; FeAsO4·0.75H2O) and basic ferric arsenate sulfate (BFAS; Fe[(AsO4)1–x(SO4)x(OH)x]·wH2O), J. Raman Spectrosc. 41 (2010) 212–221, https://doi.org/10.1002/JRS.2419.
[73] R. Betz, C. McCleland, H. Marchand, IUCr, The monoclinic polymorph of dimethylarsinic acid, Urn:Issn:1600-5368. 67 (2011) m1013–m1013. doi:10.1107/S1600536811025505.
[74] C. Luvonga, C.A. Rimmer, L.L. Yu, S.B. Lee, Analytical methodologies for the determination of organoarsenicals in edible marine species: a review, J. Agric. Food Chem. 68 (7) (2020) 1910–1934.